

# Progressive Collapse Resistance of Posttensioned Concrete Beam-Column Subassemblages with Unbonded Posttensioning Strands

Kai Qian, M.ASCE<sup>1</sup>; Yi Liu<sup>2</sup>; Tao Yang<sup>3</sup>; and Bing Li, M.ASCE<sup>4</sup>

**Abstract:** In this study, the behavior of posttensioned reinforced concrete (PC) beam-column subassemblages subjected to the loss of a middle column is investigated experimentally. The influence of unbonded posttensioning strands (UPS) with a parabolic curve on the behavior of reinforced concrete (RC) frames to resist progressive collapse is also quantified. Test results indicated that UPS have little effect on the yield load and first peak load of frames to resist progressive collapse. However, UPS could significantly increase the ultimate load capacity of the frames because stretching of strands could provide considerable additional vertical load resistance. UPS will aggregate the damage in the beam ends near to the middle column, although they may relieve the damage in the beam ends near to the side column. Moreover, UPS may change the load-resisting mechanism of the RC frame. No reliable compressive arch action developed in PC beams to resist progressive collapse because the UPS changed the distribution of the compressive stress along the beams. In addition, the effects of span/depth ratio and effective prestress in UPS on the progressive collapse resistance of PC frames are investigated. It is found that the span-depth ratio has a significant effect on the performance of RC frames to resist progressive collapse, but not the PC frames. The effective prestress in UPS has little effects on the yield load and initial stiffness of the PC frame, but it may significantly affect the ultimate deformation capacity and ultimate load capacity of the PC frame. DOI: 10.1061/(ASCE)ST.1943-541X.0001940. © 2017 American Society of Civil Engineers.

**Author keywords:** Progressive collapse; Unbonded strands; Posttensioned concrete; Beam-column subassemblages; Load-resisting mechanism; Concrete and masonry structures.

## Introduction

Progressive collapse is a phenomenon in which initial local damage leads to a chain reaction spreading throughout a much larger portion of a structure, or even an entire structure. In general, progressive collapse is characterized by a final damage zone disproportionate to the triggered initial local damage (Ellingwood et al. 2006). Examples of such structural collapses include the disproportionate collapse of the Ronan Point apartments in London in 1968 from a gas explosion and collapse of the Alfred P. Murrah Federal Building in Oklahoma city in 1995 following a truck blast. As a result of such catastrophic aftermaths, progressive collapse has obtained much interest in structural engineering communities. Several design guidelines (GSA 2003; DoD 2009) have proposed step-by-step procedures for evaluation of the progressive

collapse risks of structures. Direct and indirect design methods are proposed in the design guidelines.

The alternative load-path method (one of the direct methods) is frequently used for design because it is independent of initial damage. The objective of the method is to evaluate whether the remaining structure could generate a reliable alternate load path to redistribute the force and prevent propagation of damage. A series of experimental studies (Sasani and Kropelnicki 2008; Yi et al. 2008; Su et al. 2009; Sadek et al. 2011; Choi and Kim 2011; Qian and Li 2013; Yu and Tan 2013; Qian et al. 2015; Qian and Li 2015a, b, c; Ren et al. 2016) has been carried out for appraising the load-redistribution capacity of non-prestressed RC frames subjected to the loss of columns located in varying positions. These studies significantly improved the understanding of the behavior of reinforced concrete (RC) frames to resist progressive collapse.

However, few studies have reported on the progressive collapse behavior of posttensioned concrete (PC) frames, either from an analytical or experimental perspective. Kim and Shin (2013) evaluated the efficiency of external prestressing strands for enhancement of progressive collapse resistance of RC frames based on numerical simulation. Moreover, Kim and Choi (2015) experimentally assessed the strengthening efficiency of applying bonded or unbonded strands to improve the behavior of RC frames in resisting progressive collapse. Because PC is frequently used in buildings with high requirements in terms of durability or span length and because posttensioning strands may change the load-resisting mechanism and failure modes of the frames significantly, it is necessary to investigate the behavior of PC frames to resist progressive collapse. For this purpose, a series of PC beam-column subassemblages with unbonded posttensioning strands (UPS) is designed and tested in the present study.

<sup>1</sup>Professor, College of Civil Engineering and Architecture, Guangxi Univ., Nanning 530004, China. E-mail: qiankai@gxu.edu.cn

<sup>2</sup>Ph.D. Candidate, College of Civil Engineering and Architecture, Guangxi Univ., Nanning 530004, China. E-mail: yeah@whu.edu.cn

<sup>3</sup>Associate Professor, College of Civil Engineering and Architecture, Guangxi Univ., Nanning 530004, China. E-mail: yangt@gxu.edu.cn

<sup>4</sup>Associate Professor, School of Civil and Environmental Engineering, Nanyang Technological Univ., Singapore 639798 (corresponding author). E-mail: cbli@ntu.edu.sg

Note. This manuscript was submitted on February 22, 2017; approved on July 13, 2017; published online on November 14, 2017. Discussion period open until April 14, 2018; separate discussions must be submitted for individual papers. This paper is part of the *Journal of Structural Engineering*, © ASCE, ISSN 0733-9445.

**Table 1.** Corelationship between Prototype Frames and Corresponding Test Models

Test identifier	Prototype frame				Test model			
	Middle column (mm × mm)	Side column (mm × mm)	Beam (mm × mm)	Diameter of strands (mm)	Middle column (mm × mm)	Side column (mm × mm)	Beam (mm × mm)	Diameter of strands (mm)
RCS	500 × 500	500 × 500	500 × 300	N/A	250 × 250	400 × 400	250 × 150	N/A
RCL	500 × 500	500 × 500	500 × 300	N/A	250 × 250	400 × 400	250 × 150	N/A
PCS-0.4	500 × 500	500 × 500	500 × 300	17.8	250 × 250	400 × 400	250 × 150	12.7
PCS-0.6	500 × 500	500 × 500	500 × 300	17.8	250 × 250	400 × 400	250 × 150	12.7
PCL-0.4	500 × 500	500 × 500	500 × 300	17.8	250 × 250	400 × 400	250 × 150	12.7

**Table 2.** Specimen Properties

Test identifier	Beam section (mm × mm)	Beam clear span (mm)	Diameter of posttensioning strands (mm)	Effective prestress	Top (bottom) beam longitudinal rebar ratio $\rho$	Axial force in middle column (kN)
RCS	150 × 250	2,750	N/A	N/A	0.7% (0.7%)	−25
RCL	150 × 250	3,300	N/A	N/A	0.7% (0.7%)	−30
PCS-0.4	150 × 250	2,750	12.7	$0.4f_{pu}$	0.7% (0.7%)	−25
PCS-0.6	150 × 250	2,750	12.7	$0.6f_{pu}$	0.7% (0.7%)	−25
PCL-0.4	150 × 250	3,300	12.7	$0.4f_{pu}$	0.7% (0.7%)	−30

Note: Reinforcement ratios were determined using equation  $\rho = A_s/bd_0$ , in which  $b$  and  $d_0$  represent the width and effective depth of beam cross sections; and  $f_{pu}$  is the ultimate strength of the strands.

## Experimental Program

### Specimen Design

To experimentally investigate the structural behavior of PC frames with UPS subjected to the loss of a middle column, a series of beam-column subassemblages, including two nonprestressed RC specimens (for reference) and three PC specimens with UPS, were constructed and tested. The specimens are one-half-scaled in consideration of the capacity of the test facilities. Table 1 gives the corelationship between prototype frame and scaled models, and Table 2 presents key details of the test specimens. Fig. 1(a) illustrates the dimensions and reinforcement details of Specimen PCS-0.4. The designation of PCS-0.4 represents a PC specimen that has effective prestress ( $f_{pe}$ ) of  $0.4f_{pu}$  and span/depth ratio of 12 (short span).

As shown in Fig. 1, two beams, one middle-column stub, and two enlarged side-column stubs were cast monolithically. The cross section of the beam was  $250 \times 150 \text{ mm}^2$ , and the cross section of middle column was  $250 \times 250 \text{ mm}^2$ . The side column stubs were enlarged to  $400 \times 400 \text{ mm}^2$  for applying fixed boundary conditions. The installed top and bottom longitudinal reinforcement of PCS-0.4 was 3T10, which corresponds to a reinforcement ratio of 0.7%. The rebar was installed in the beam continuously and anchored to the side-column stubs with  $90^\circ$  hooks. The transverse reinforcement in the reinforced zone and remaining zone was R6 at 50 mm and R6 at 100 mm, respectively, to simulate seismic design details. T10 and R6 represent deformed rebar with diameter of 10 mm and plain rebar with diameter of 6 mm, respectively. UPS with a nominal diameter of 12.7 mm was installed in the beam with a parabolic curve. The UPS were twisted by seven wires with nominal area of  $98 \text{ mm}^2$ . The parabolic profile of UPS in the beam satisfies Eqs. (1) and (2)

$$y_1 = 0.12x_1^2 \quad (1)$$

$$y_2 = 0.28x_2^2 \quad (2)$$

where  $y_1$  = vertical coordinate of the strand from the origin in the middle of the beam;  $x_1$  = horizontal coordinate of the strand from

the origin in the middle of the beam;  $y_2$  = vertical coordinate of the strand from the origin in the center of the middle column; and  $x_2$  = horizontal coordinate of the strand from the origin in the center of the middle column.

PCS-0.6 has identical dimensions and reinforcement details as PCS-0.4, but higher effective prestress  $0.6f_{pu}$  in the UPS. As shown in Fig. 1(b), PCL-0.4 has similar dimensions and reinforcement details as PCS-0.4. However, it has a longer design span of 3,500 mm and span/depth ratio of 14. Similar to PCS-0.4, an effective prestress  $0.4f_{pu}$  was applied before tests. The key design details of the specimens are tabulated in Table 2. For non-prestressed RC specimens RCS and RCL (control specimens), similar dimensions and reinforcement details as PCS-0.4 and PCL-0.4, respectively, were used, but no UPS were installed.

### Material Properties

All specimens were constructed using ready-mixed concrete, which had a design cylinder compressive strength of 40 MPa. Average cylinder compressive strengths measured on the days of testing for Specimens PCS-0.4, PCS-0.6, PCL-0.4, RCS, and RCL were 44.1, 43.2, 44.8, 43.6, and 43.9 MPa, respectively. Grade 300 (R6) and Grade 400 (T10) steel bars were used as transverse reinforcement and longitudinal reinforcements, respectively. Low-relaxation posttensioning strands were used to apply posttensioning force in the beams. Table 3 tabulates the material properties of the nonprestressed reinforcements and the strands.

### Test Setup

For simplicity, a test setup (Fig. 2) commonly used for pushdown tests in previous studies (Sasani and Kropelnicki 2008; Su et al. 2009; Choi and Kim 2011; Lu et al. 2017; Ren et al. 2016) was used. In those previous tests, the middle column was removed first before applying the concentrated force at the assumed lost column. Thus, the effects of uniformly distributed service load are ignored. To reflect more realistic frame behavior, the uniformly distributed service load and release of the initial axial force in the middle column are simulated in this study.

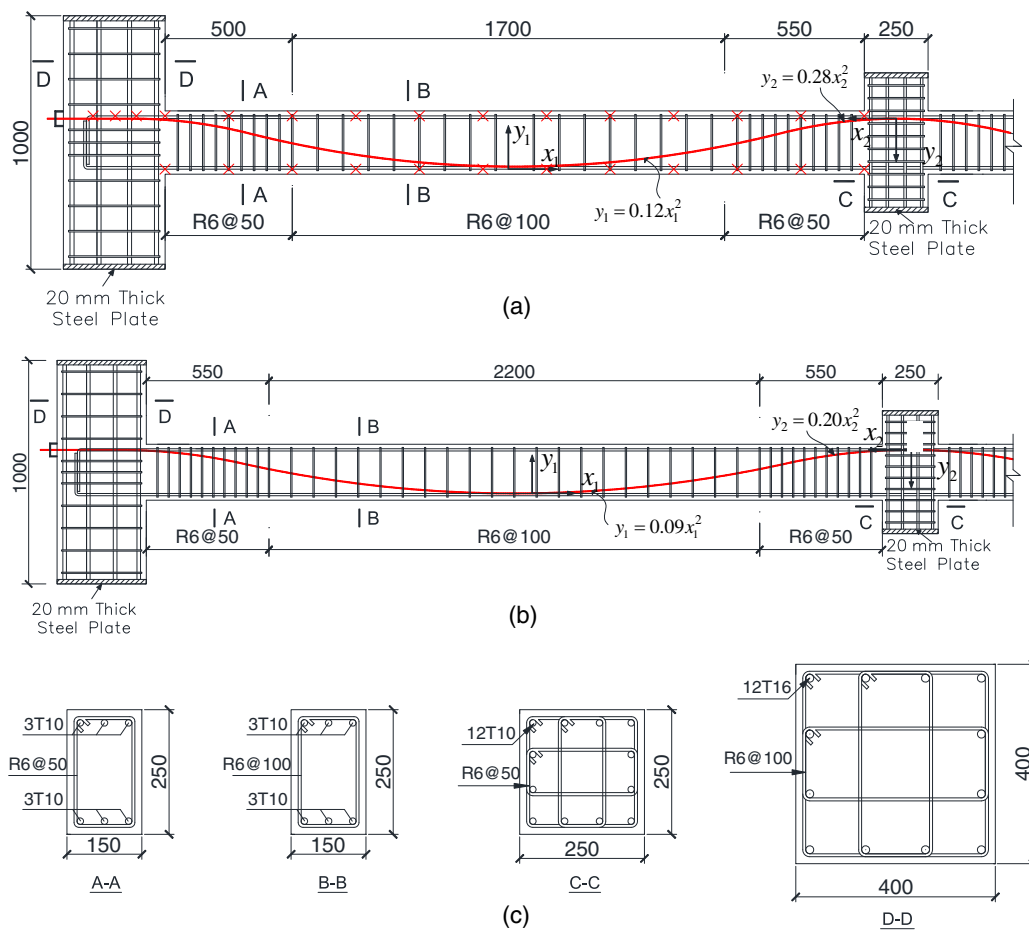


Fig. 1. Dimensions and reinforcement details of typical prestressed specimens: (a) PCS-0.4; (b) PCL-0.4; (c) cross sections

Table 3. Material Properties of Reinforcement and Unbonded Posttensioning Strands

Item	Nominal diameter (mm)	Yield strength (MPa)	Ultimate strength (MPa)	Elongation (%)
Transverse reinforcement R6	6	372	510	19.5
Longitudinal reinforcements T10	10	455	635	22.8
Posttensioning strands	12.7	1,650	1,860	6.1

Note: R6 represents a plain bar of with diameter of 6 mm; T10 represents deformed rebar with diameter of 10 mm.

Fig. 3 illustrates the test setup of a typical PC specimen before removal of the middle column. As shown in the figure, fixed boundary conditions were applied to the side columns by two horizontal constraints and a pin connection. To eliminate horizontal constraints from the pin connection, a series of steel rollers were set below the pin connection. A hydraulic jack [Item 3 in Fig. 3(a)] was installed below the middle column to release the axial force manually. The stroke of the jack [Item 3 in Fig. 3(a)] initially protruded to touch the bottom of the middle column to simulate the middle column being intact. Then, a series of six steel-weight assemblages [Item 6 in Fig. 3(a)] were hung below the beams to simulate the

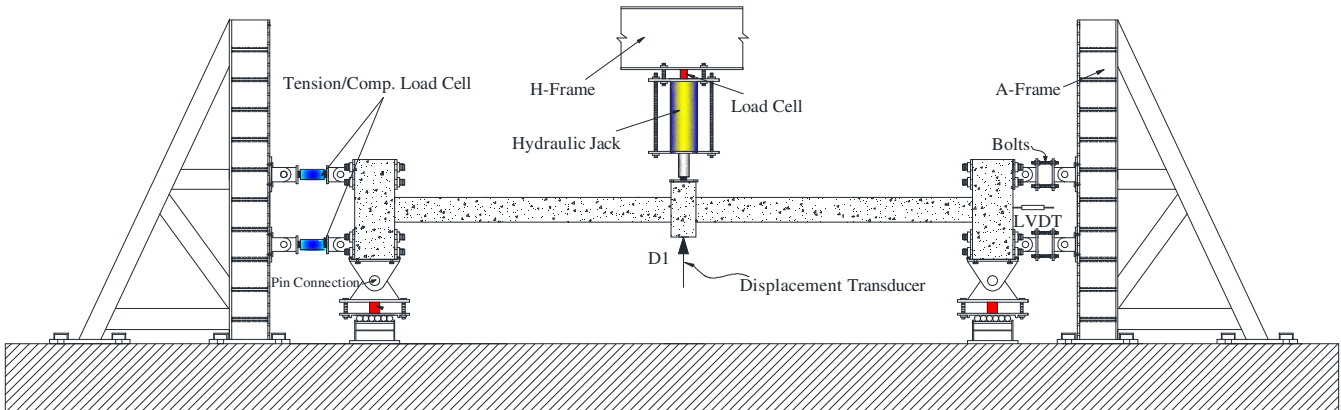
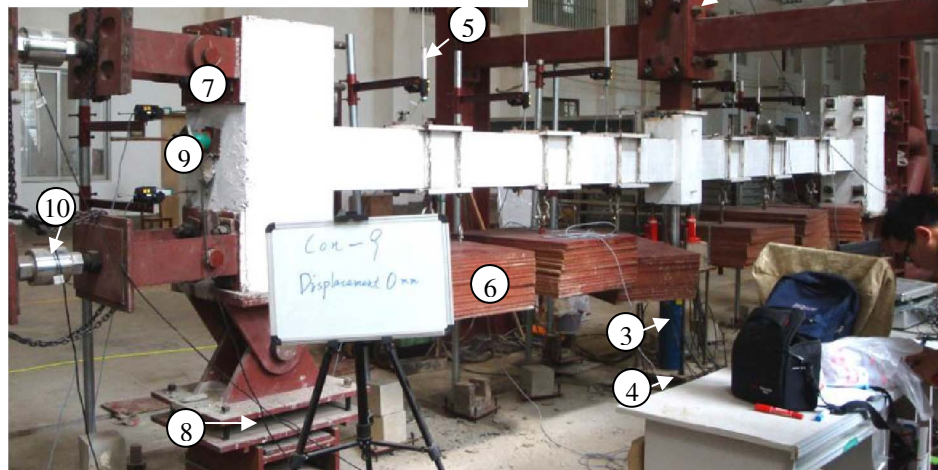
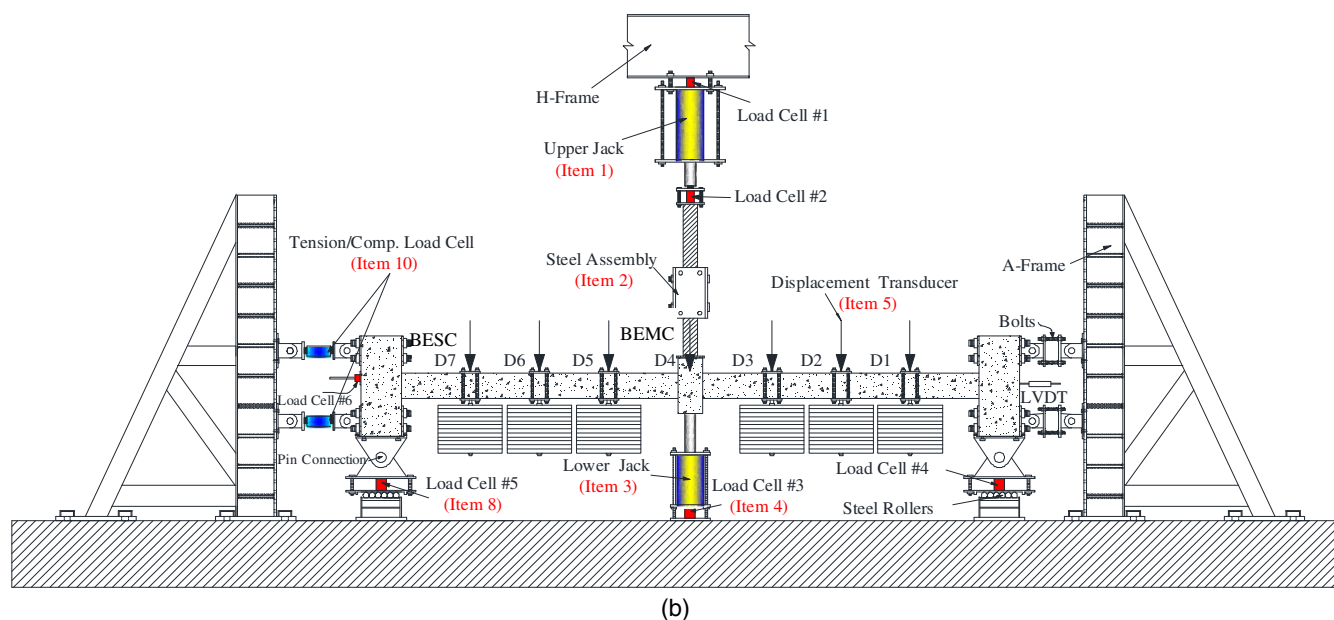


Fig. 2. Test setup and instrumentation layout in simplified pushdown tests

- |                            |                             |
|----------------------------|-----------------------------|
| 1. Upper Jack              | 6. Steel Weights            |
| 2. Steel Assemble          | 7. Displacement Transducer  |
| 3. Lower Jack              | 8. Load Cell                |
| 4. Load Cell               | 9. Load Cell                |
| 5. Displacement Transducer | 10. Tension/comp. Load Cell |



(a)



(b)

**Fig. 3.** Test setup and instrumentation layout: (a) photograph; (b) schematic view

design service load. Once the weights were hung completely and the instruments ready to record the data, the stroke of the lower jack [Item 3 in Fig. 3(a)] was retracted gradually to simulate a slow release of the axial force in the middle column. If the specimen could stabilize after the stroke of the lower jack completely detached from the middle column, the stroke of the upper jack [Item 1 in Fig. 3(a)] began to protrude to apply additional force on the middle column until failure. To eliminate out-of-plane failure of the two-dimensional (2D) beam-column subassemblages, a specially designed steel assembly [Item 2 in Fig. 3(a)] was installed below the upper jack. The steel assembly consisted of a steel box and several steel pins to allow only vertical movement of the middle column but constrain its rotation and horizontal movements.

### Instrumentation

A series of instruments were installed internally and externally to monitor the behavior of test specimen during tests. As shown in Fig. 3(b), two load cells were installed below or above the upper jack to measure the additional axial force applied on the middle column in case the design service load does not lead to specimen failure. A load cell [Item 4 in Fig. 3(a)] was installed below the lower jack to measure the initial axial force in the middle column and monitor the releasing of the axial force during the tests. Load cells [Item 8 in Fig. 3(a)] were also installed below the pin connection of each side column to monitor the load redistribution during the tests. Moreover, a load cell [Item 9 in Fig. 3(a)] was installed at the end of the strands to monitor the prestressing force



in the strands. Two tension/compression load cells [Item 10 in Fig. 3(a)] were installed in the horizontal constraints to monitor the horizontal reaction force applied on the side column. A series of seven displacement transducers [Item 5 in Fig. 3(a)] were installed

to measure the deformation shape of the specimens. Strain gauges were attached to the nonprestressed reinforcements before casting.

## Experimental Results

Five specimens were tested by pushdown loading regime to study the behavior of PC frames to resist progressive collapse. The efficiency of internal installed UPS for upgrading the progressive collapse resistance of RC frames was also evaluated by comparison of the performance of PC specimens and the corresponding nonprestressed RC specimens. The test results are discussed in the following subsections.

### Global Behavior and Failure Modes

#### Control Specimen RCS

The Control Specimen RCS had a beam span/depth ratio of 12. Fig. 4(a) shows the vertical load-vertical displacement of the control specimens. Fig. 4(a) depicts the vertical load-vertical displacement of the control specimens. As shown in the figure, after applying 5-t weights the beams, the initial axial force measured in the lower jack was approximately  $-25$  kN. For easy comparison of specimens' performance, the load-displacement curves are shifted from  $(0, -25)$  to origin  $(0, 0)$ . Taking Specimen RCS as an example, the stage from 0 to 25 kN in the shifted curve represents the phase of initial axial force releasing in the original curve. The load-displacement curves of the remaining specimens shown in the figure are given after shifting. The values in Table 4 are also selected from the shifted curves. For Specimen RCS, when the axial force increased to 25 kN, the vertical displacement of the middle column (DMC) measured 34 mm, and the stroke had completely detached from the bottom of middle column.

To measure the failure mode and load-resisting capacity of the specimen, additional axial force was applied by the upper jack. If increasing the vertical load to 32 kN, first yielding was observed in the beam's longitudinal reinforcement. Further increasing the DMC to 67 mm, a first peak load (FPL) of 44 kN was measured. After that, concrete crushing occurred in the compression zone of the beam end near to the side column (BESC). The load-resisting capacity slightly decreased until the displacement reached 172 mm. After that, the load-resisting capacity began to reascend because of the development of catenary action in the beams. When the displacement reached 436 mm, rebar fracture occurred in the BESC.

The ultimate load (UL) capacity of the specimen in the large displacement stage was measured as 68 kN. No rebar fracture was observed in the beam end near the middle column (BEMC), which is quite different from previous tests (Sasani and Kropelnicki 2008; Yi et al. 2008; Su et al. 2009; Sadek et al. 2011; Choi and Kim 2011; Yu and Tan 2013; Qian et al. 2015; Ren et al. 2016). In those tests, rebar fracture was first observed in the BEMC when the vertical displacement reached approximately  $0.1l_n$ , where  $l_n$  is the

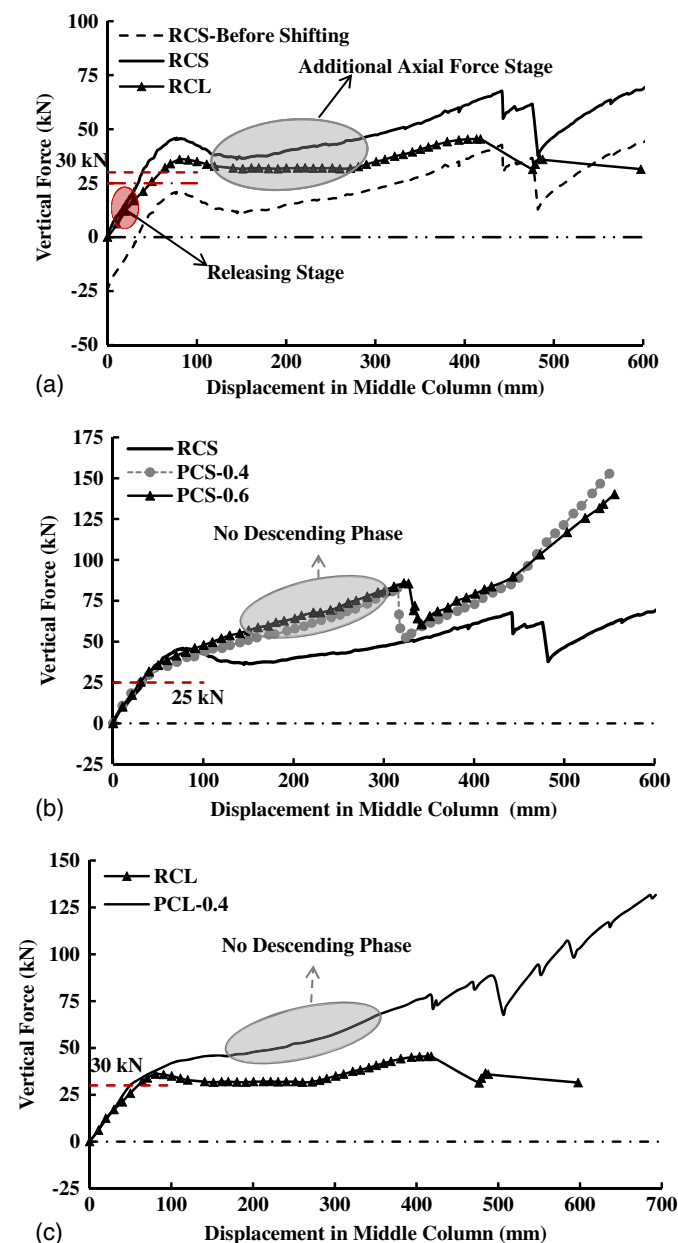


**Fig. 4.** Comparison of the load-displacement curves: (a) control specimens; (b) specimens with low span/depth ratio; (c) specimens with high span/depth ratio

**Table 4.** Test Results

Specimen identifier	Critical displacement (mm)				Critical load (kN)			Maximum horizontal tensile force (kN)	Maximum incremental prestress (MPa)
	Full release of axial force	First yield load	First peak load	Ultimate load	First yield	First peak load	Ultimate load		
RCS	34	40	67	598	32	44	68	153	N/A
RCL	59	46	80	413	25	36	45	135	N/A
PCS-0.4	32	40	N/A	550	30	N/A	153	336	1,184
PCS-0.6	25	40	N/A	556	32	N/A	140	323	814
PCL-0.4	50	60	N/A	692	33	N/A	131	303	1,154

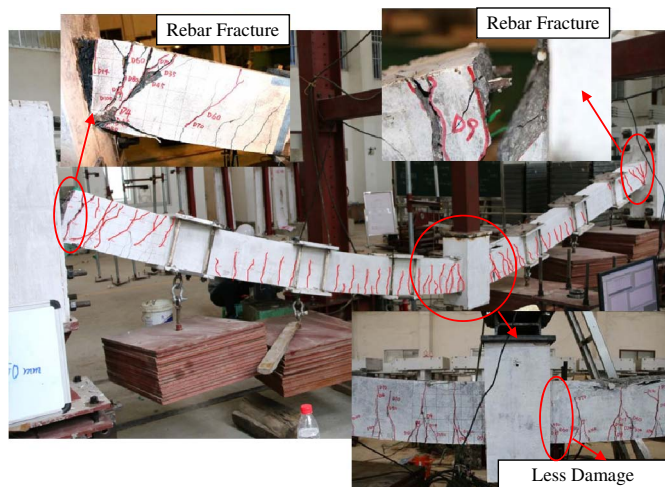


Fig. 5. Failure mode of Specimen RCS

clear span of the beam. This is because a simplified pushdown loading regime excluded design service loads (no uniformly distributed weights applied on the beams) was carried out in those tests. Thus, the rotation and damage were concentrated in the beam ends. Moreover, the beams were deformed almost straight in the stage of catenary action. However, as shown in Fig. 5, the failure mode of RCS indicated that the beams are deformed in curves. The damage in the BEMC was evenly distributed in a region with  $0.18l_n$  length. Because buildings have considerable uniformly distributed service load in reality, the test setup proposed in this study is more realistic.

**Control Specimen RCL.** The Control Specimen RCL had beam span/depth ratio of 14. As shown in Fig. 4(a), different to RCS, an initial axial force of  $-30$  kN was measured in the lower jack because of the longer design span. After shifting of the load-displacement curve, the yielding of the beam's longitudinal reinforcement was measured when the vertical load increased to  $25$  kN. Further increasing the vertical load to  $30$  kN, the lower jack was detached from the middle column and the measured DMC was

$59$  mm, which is approximately  $173\%$  of that in RCS. Then, the upper jack began to apply additional force. When the vertical force increased to  $36$  kN, the DMC was measured as  $80$  mm. With further increments of vertical force, the DMC increased dramatically until it reached  $272$  mm. At that stage, concrete crushing was severe in the compression zone of BESC. Increases in load-resisting capacity were observed when the DMC was further increased. When the vertical displacement reached  $413$  mm, rebar fracture occurred in the BESC. The UL capacity of  $45$  kN was measured at this displacement stage. The failure mode of this specimen is illustrated in Fig. 6. As shown in the figure, similar to RCS, rebar fracture was observed in the BESC but not in the BEMC. Compared with BESC, the cracks that developed in the BEMC are much thinner.

**PC Specimen PCS-0.4.** Specimen PCS-0.4 had a similar span/depth ratio as RCS, but included UPS with a nominal diameter of  $12.7$  mm. Similar to RCS, the measured initial axial force in the lower jack was approximately  $-25$  kN. Different from RCS, no cracks were observed in the beams when  $5$ -t weights were completely applied to the beams. Moreover, the DMC measured  $32$  mm when the vertical force increased to  $25$  kN and the lower jack was completely detached from the bottom of the middle column. When the vertical force increased to  $30$  kN, yielding was observed in the beam longitudinal reinforcements. Thus, the UPS did not increase the yield load capacity of the specimen significantly because the existing profile of the strands are designed to resist gravity loads, which may result in negative effects in the BENM even after removal of the middle column because of bending moment reversal. Strands with different profiles might be designed if progressive collapse resistance is the main concern in design, as suggested by Kim and Shin (2013).

When the DMC increased to  $50$  mm, concrete crushing first occurred in the BEMC, which is different from that of RCS. Moreover, cracks in BEMC were much wider than those in BESC. Further increasing the displacement to  $311$  mm, rebar fracture was observed in the BEMC, which is also quite different from that in RCS. For safety, the test was stopped at a vertical displacement of  $550$  mm because the measured stress in UPS had reached its ultimate strength. The measured UL capacity of this specimen was

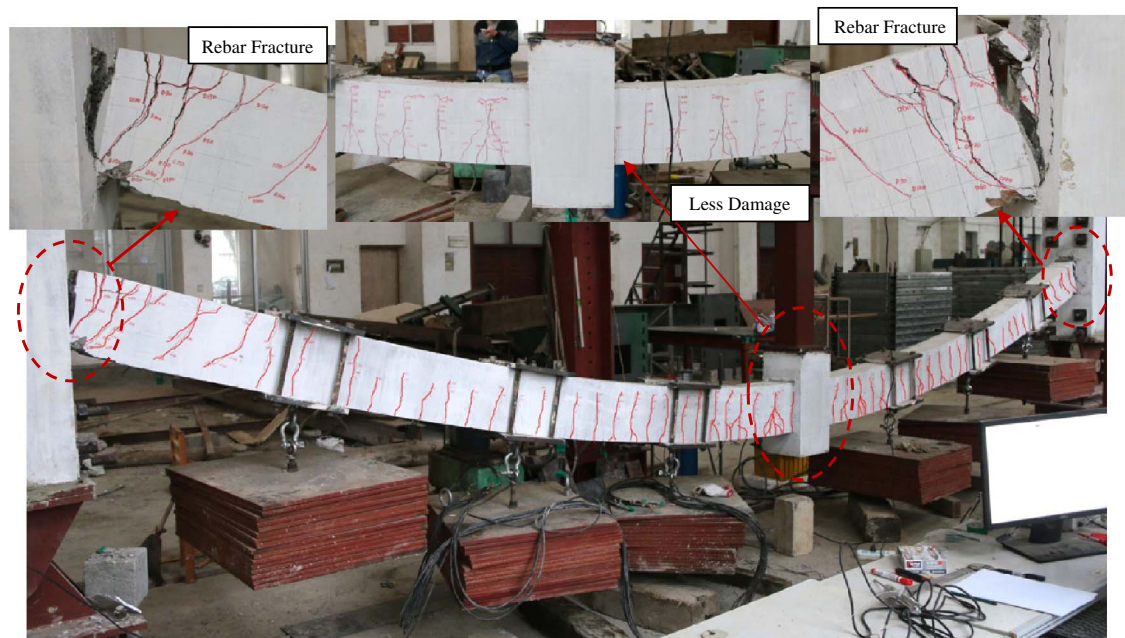


Fig. 6. Failure mode of Specimen RCL



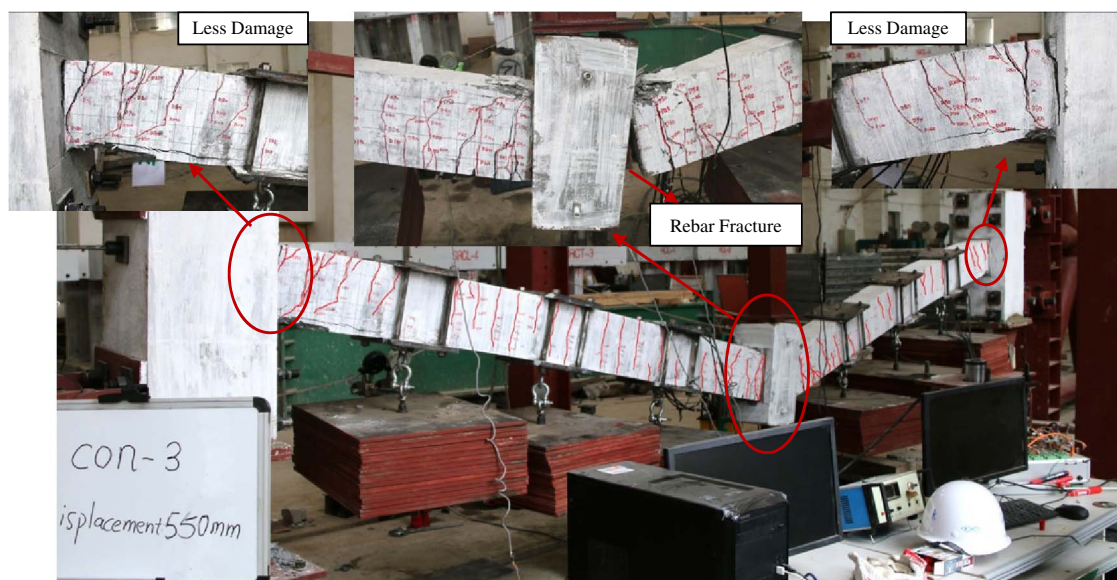


Fig. 7. Failure mode of Specimen PCS-0.4

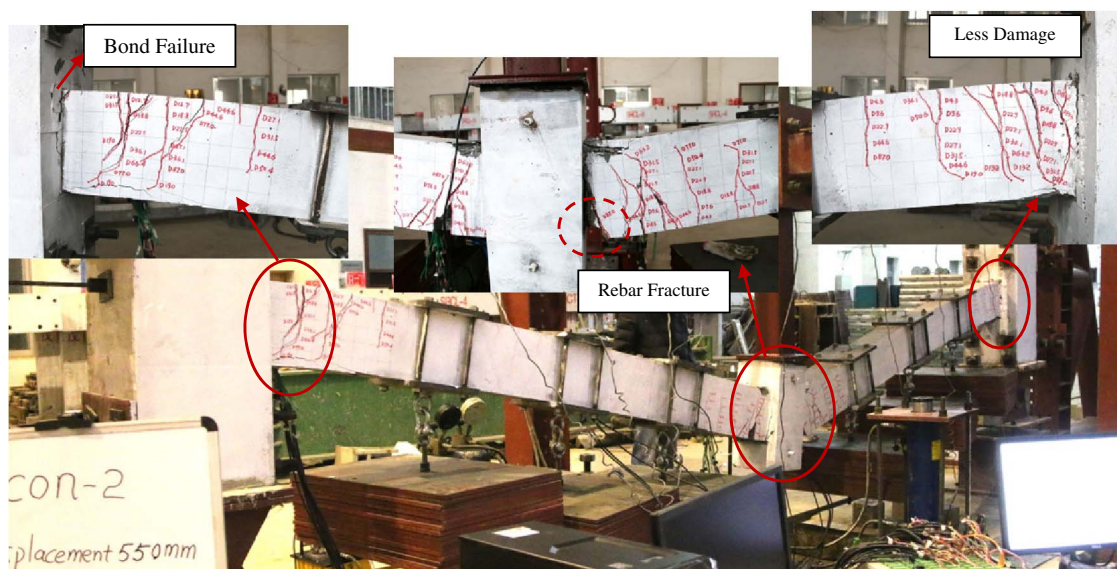


Fig. 8. Failure mode of Specimen PCS-0.6

153 kN, which is approximately 225% of that of RCS. Fig. 7 illustrates the failure mode of PCS-0.4. As shown in the figure, rebar fracture is only observed in BEMC (different from RCS). No wide cracks were observed in the BESC. The UPS did not fracture at displacement of 550 mm. Different from Specimen RCS, the deformation of the beams in PCS-0.4 was almost straight in the final stage.

**PC Specimen PCS-0.6.** Specimen PCS-0.6 had similar dimensions and reinforcement details as PCS-0.4, but higher effective prestress of  $0.6f_{pu}$ . In general, the behavior and failure mode of this specimen were similar to those of PCS-0.4. The main difference between these two specimens is emphasized herein. The first yield was observed in the beam longitudinal reinforcement at a vertical load of 32 kN. When the DMC reached 320 mm, rebar fracture was first observed in the BEMC. The UL capacity of the specimen was measured as 140 kN in accordance with DMC of 556 mm. The failure

mode of PCS-0.6 is illustrated in Fig. 8. Similar to PCS-0.4, rebar fracture was only observed in BEMC, and the beams were almost straight. Compared with PCS-0.4, the damage of BESC in PCS-0.6 is milder because of the higher compressive stress attributable to higher effective prestress.

**PC Specimen PCL-0.4.** Specimen PCL-0.4 had similar dimensions and reinforcement details as RCL, but included UPS with a nominal diameter of 12.7 mm. The initial axial force in the lower jack was approximately  $-30$  kN after applying the weights. Similar to PCS-0.4, no cracks were observed in the beams after applying the weights. When the vertical force increased to 13 kN, cracks were observed in the bottom of the middle beam. After further increases in vertical force to 22 kN, cracks also occurred in the BEMC. When the vertical load increased to 30 kN, cracks began to form in the BESC. Further increasing the vertical load, more and more cracks formed in the beams. The yield load of 33 kN was reached at a DMC

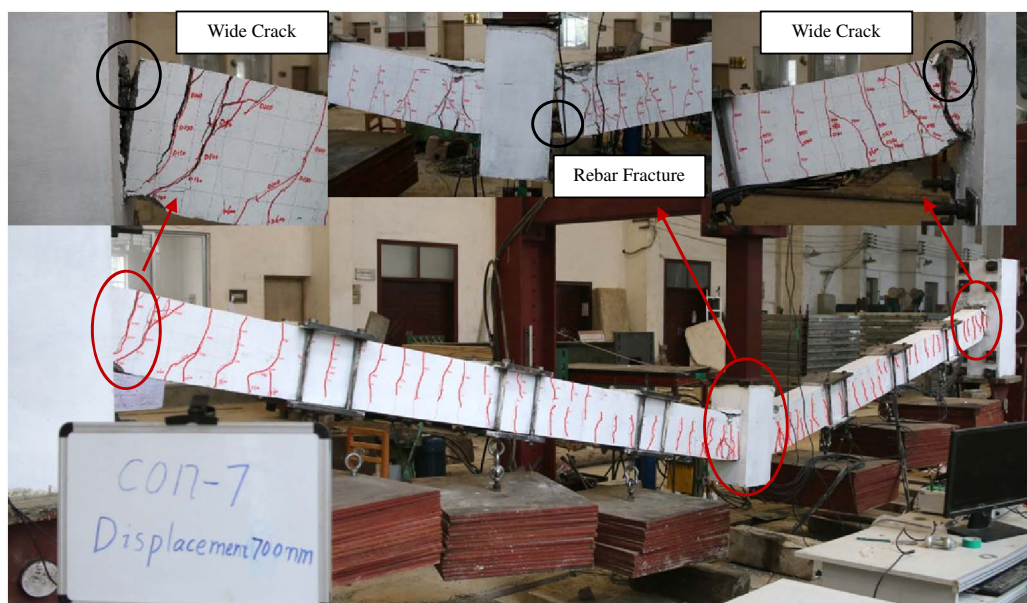


Fig. 9. Failure mode of Specimen PCL-0.4

of 60 mm. However, cracks in BEMC were much wider than those in BESC, which is quite different from those in RCL.

When the DMC increased to 120 mm, concrete crushing was first observed in the BEMC. Moreover, rebar fracture was first observed in the BEMC at a DMC of 493 mm. When the DMC reached 692 mm, rebar fracture also occurred in the BESC. The UL capacity of this specimen was measured as 131 kN, which is approximately 291% of that of RCL. The failure mode of PCL-0.4 is shown in Fig. 9. As shown in the figure, compared with PCS-0.4, the damage in the BESC is more severe. However, similar to PCS-0.4, the beams deformed in a straight manner.

### Horizontal Reaction Force

Fig. 10 illustrates the horizontal reaction force versus vertical displacement in the middle column. As shown in the figure, for Specimens RCS and RCL, considerable compressive force is initially measured in the horizontal constraints. The maximum compressive force in RCS and RCL was  $-139$  and  $-154$  kN, respectively. The compressive force of RCS and RCL began to reduce when the vertical displacement exceeded 75 and 90 mm, respectively. For both specimens, the tensile force was observed in large displacement stages. The maximum tensile force measured in RCS and RCL was 153 and 135 kN, respectively. For PC specimens, the response

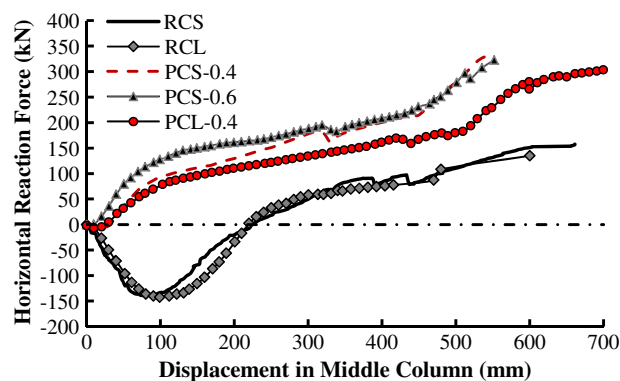


Fig. 10. Horizontal reaction force versus vertical displacement in middle column

of horizontal reaction force was quite different from that of RC specimens.

No compressive force was measured in PC specimens during the tests. This could be explained by the UPS changing the distribution of the compressive stress in the beams. As shown in Fig. 11, in non-prestressed RC specimens, compressive struts could have developed in RC beams to directly distribute the vertical force to side column. However, the UPS in PC specimens will relieve the compressive stress in the BESC but aggravate the compressive stress in BEMC. Thus, no reliable compressive struts could develop in PC beams to directly transfer the vertical force, which agrees well with the failure mode of the PC specimens.

As shown in Figs. 7–9, for PC specimens, concrete crushing is only severe in BEMC when the displacement is less than  $0.1l_n$ . The measured maximum horizontal reaction force in PCS-0.4 and PCL-0.4 was 336 and 303 kN, which is 220 and 224% of that of RCS and RCL, respectively. For PCS-0.6, the maximum horizontal reaction force was 323 kN, which is approximately 211% of that of RCS. The greater horizontal reaction force in PC specimens was attributable to the tension of UPS in the large deformation stage. The measured tensile stress in UPS during tests is shown in Fig. 12. As shown in the figure, the strands in PC specimens have yielded. The measured ultimate stress in UPS of PCS-0.4, PCS-0.6, and PCL-0.4 was 1,902, 1,893, and 1,889 MPa, respectively. Tests were terminated mainly because the measured stress in UPS had exceeded their nominal ultimate strength.

### Deformation Shape

Fig. 13 shows the deformation shape of the beams in different stages: releasing the axial force completely, first yield of the beam rebar, peak load capacity, DMC reaching 100 and 200 mm, and ultimate load capacity. As shown in Fig. 13(a), for Specimen RCS, the deformation of the beams is curved until failure. The chord rotation, which is defined as the ratio of DMC to the clear span of the beam by the U.S. Department of Defense (DoD) (DoD 2009), will slightly overestimate the rotation of the BESC but significantly underestimate the rotation in BEMC. Moreover, the deformation of the beams is quite different from that observed in beams tested in previous studies (Sasani and Kropelnicki 2008; Yi et al. 2008; Su et al. 2009; Sadek et al. 2011; Choi and Kim 2011).



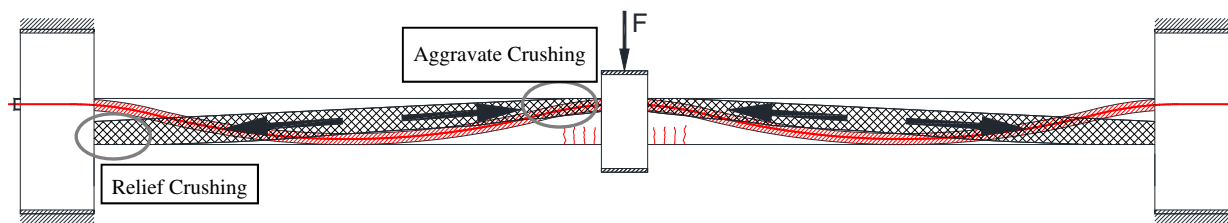


Fig. 11. Schematic explanation of the limit compressive arch action in PC specimens

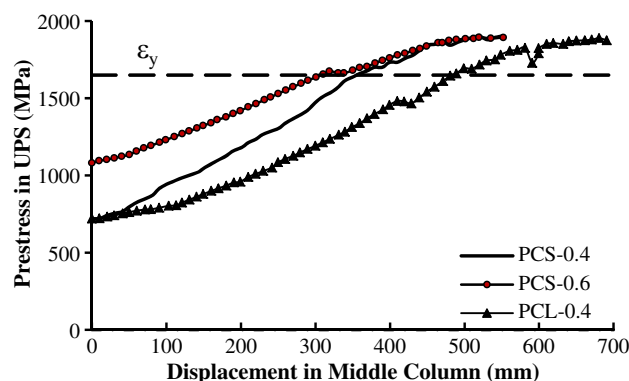


Fig. 12. Prestress in UPS versus vertical displacement in middle column

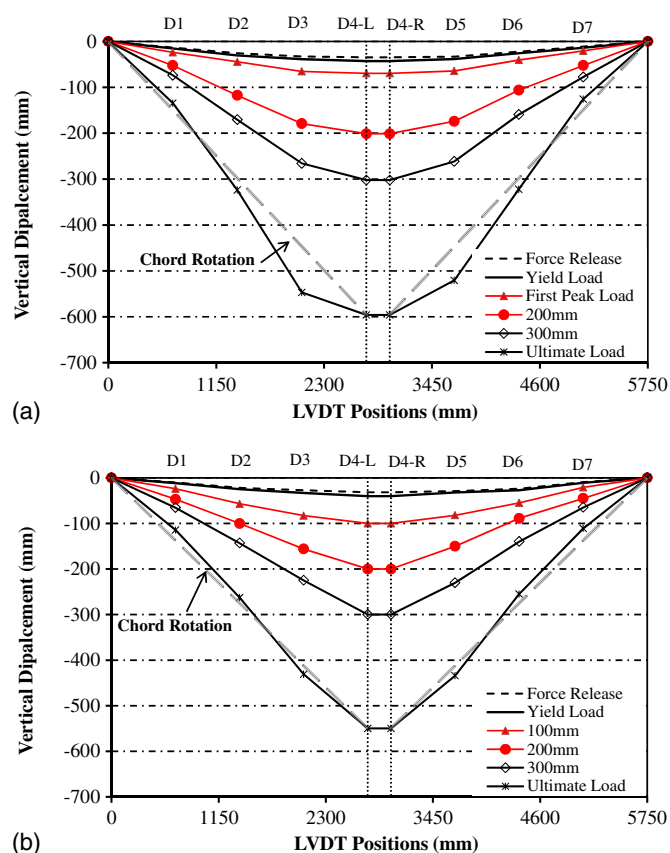


Fig. 13. Deformation shape of the beams: (a) Specimen RCS; (b) Specimen PCS-0.4

However, for Specimen PCS-0.4, the deformation of the beam was curved only at the stage of just releasing the axial force completely. After the DMC reached  $0.05l_n$ , the beams were deformed in a straight manner, which could be explained by the double action of the uniformly distributed weights and reversed arch action of the UPS in the BEMC. As shown in Fig. 14, the vertical component of the prestressing force in the UPS will aggravate the damage in the BEMC. Although the chord rotation defined by DoD (2009) is for RC beams, it was found that chord rotation is more accurate for PC beams than for RC beams.

### Strain-Gauge Results

Fig. 15 shows the strain distribution in the longitudinal reinforcement of Specimen RCS. As shown in Fig. 15(a), before removal of the middle column, considerable tensile stress was measured in the top reinforcement near the side column and middle column, whereas compressive stress was measured in the middle part of the beam. After removal of the middle column, the tensile stress in the beam longitudinal reinforcement near to the side column dramatically increased, whereas compressive stress was measured in the beam longitudinal reinforcement near to the middle column. Thus, bending moment reversal occurred in the BEMC after removal of the middle column. Similar behavior is also observed in the bottom beam longitudinal reinforcement in Fig. 15(b). As can be seen from the figure, the top longitudinal reinforcement in the BESC yields earlier than the bottom longitudinal reinforcement in BEMC. In the UL stage, the whole top reinforcement is almost in tension.

Fig. 16 shows the strain distribution along the beam longitudinal reinforcement of PCS-0.4. As shown in the figure, the initial strain in the beam longitudinal reinforcement of PCS-0.4 is much smaller than that in RCS. Similar to RCS, bending moment reversal occurred in the BEMC after removal of the column. However, different from RCS, for PCS-0.4, yielding first occurred in bottom reinforcement in the BEMC, rather than the top reinforcement in the BESC. Moreover, the tensile stress developed in the top longitudinal reinforcement of PCS-0.4 was much slower. For the remaining specimens, similar results were observed.

### Discussion of the Test Results

#### Effects of Span/Depth Ratio

As indicated in Fig. 4 and Table 4, compared with Specimen RCL, Specimen RCS achieved greater yield load capacity and UL capacity by 28 and 51%, respectively. However, the yield load capacity and UL capacity of PC Specimen PCS-0.4 are only approximately 91 and 117% of that of PCL-0.4. Thus, the span/depth ratio has greater effects on the RC frames than that on the PC frames, especially for UL capacity. As shown in Figs. 5–7 and 9, the span/depth ratio has little effect on the failure mode of RC and PC specimens.

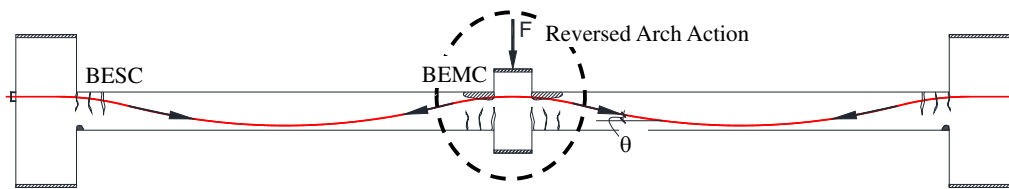


Fig. 14. Schematic illustration of the reversed arch action in the BEMC

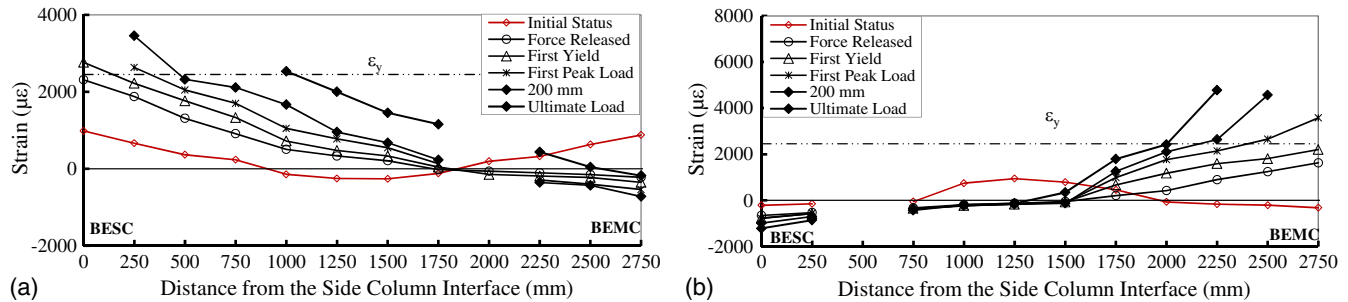


Fig. 15. Strain distribution in longitudinal reinforcement of Specimen RCS: (a) top rebar; (b) bottom rebar

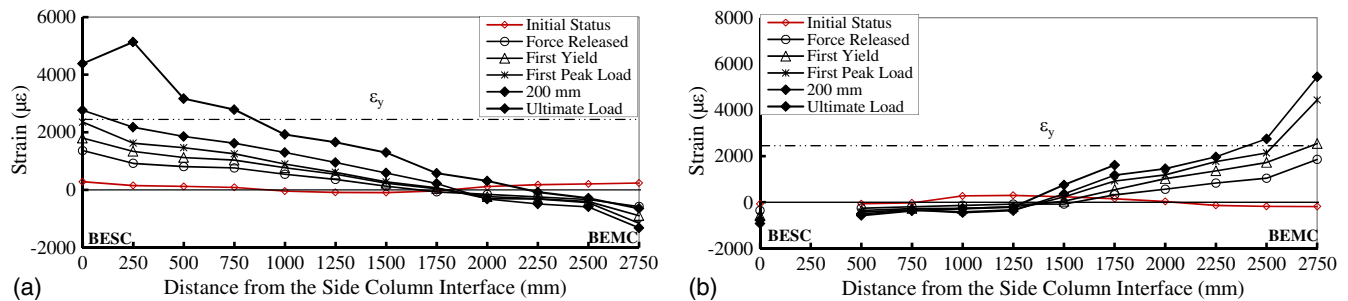


Fig. 16. Strain distribution in longitudinal reinforcement of Specimen PCS-0.4: (a) top rebar; (b) bottom rebar

### Effects of Effective Prestress in UPS

As shown in Fig. 4(b), generally, the behavior of PCS-0.6 is very similar to that of Specimen PCS-0.4. The yield load capacity of PCS-0.6 and PCS-0.4 is 32 and 30 kN, respectively. Thus, the effective prestress in UPS had little effect on the initial stiffness and yield load capacity. As listed in Table 4, the UL capacity of PCS-0.6 and PCS-0.4 is 140 and 153 kN, respectively. This is because the UPS in PCS-0.6 yielded earlier than those in PCS-0.4. For similar reasons, a higher horizontal reaction force was measured in PCS-0.4. Relatively lower effective prestress was designed in this study because the diameter of the UPS was not proportionally scaled down, reflecting material availability in the market. In practical projects, if higher effective prestress is designed in the strands (e.g.,  $0.80f_{pu}$ ), prefraction of strands may result in the specimen achieving lower ultimate deformation capacity and UL capacity. Thus, it is suggested that PC frames are designed with proper effective prestress when progressive collapse risks are a main concern in design because the benefits of UPS mainly relate to the frames' deformation ability.

### Effects of Unbonded Posttensioning Strands

Quantification of the effects of UPS on the behavior of RC frames to resist progressive collapse is one of the main objectives of this

study. As tabulated in Table 4, the measured yield load capacity of RCS and PCS-0.4 is 32 and 30 kN, respectively. Thus, UPS have little effect on the initial behavior of the frame. However, the measured UL capacity of RCS and PCS-0.4 is 68 and 153 kN, respectively. Thus, the UPS could increase the UL capacity of the frame by 125%. For RCL and PCL-0.4, UPS could increase the yield load capacity and UL capacity by 32 and 191%, respectively. Moreover, as shown in Fig. 4, no descending branch is observed in the load-displacement curves of PC specimens. As shown in Fig. 10, the response of horizontal reaction force indicated that no compressive force develops in the horizontal constraints of PC specimens. Thus, UPS will change the load-resisting mechanism of the frames to resist progressive collapse. No effective compressive arch action could develop in PC specimens to resist progressive collapse.

Furthermore, as shown in the failure modes, rebar fracture occurred in the BESC in RC specimens, but it first occurred in BEMC in PC specimens. Thus, the UPS may also change the failure mode of the frames. To identify the contribution of RC beams and UPS in the load resistance of PC specimens, the load resistance of PC specimens is decomposed. Because the dimensions and reinforcement details in RC and corresponding PC specimen are identical, it is assumed that the load resistance of the RC frame is identical to that of the RC specimen and corresponding PC specimen. Thus, in this load-resistance decomposition analysis, the difference of the load

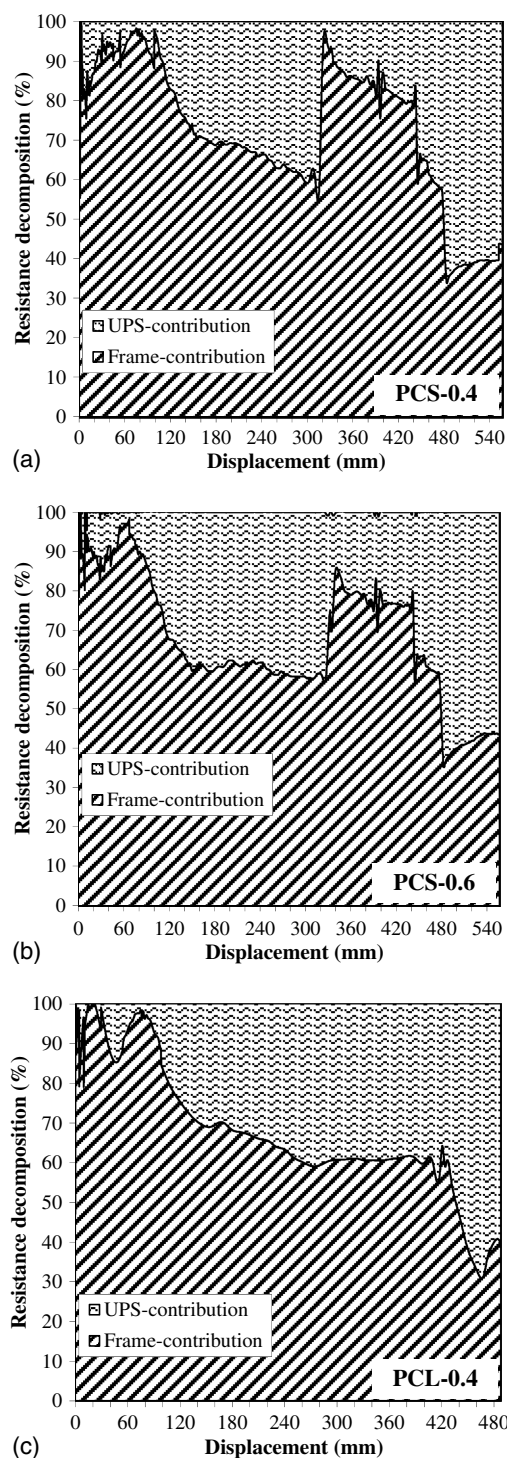


**Fig. 17.** Decomposition of load resistance of RC frame and UPS in PC specimens: (a) PCS-0.4; (b) PCS-0.6; (c) PCL-0.4

resistance between RC and corresponding PC specimen is attributed to UPS. As shown in Fig. 17, in the initial stage, majority of the load resistance (approximately 90%) is contributed by the RC frame. After yielding of the reinforcements and crushing of the concrete, the contribution of UPS increased to 40%. Moreover, after fracture of the nonprestressed reinforcements, the contribution of UPS keeps increasing. At the final stage of the test, approximately 60% of the load resistance can be attributed to the stretching of the UPS in the large deformation stage.

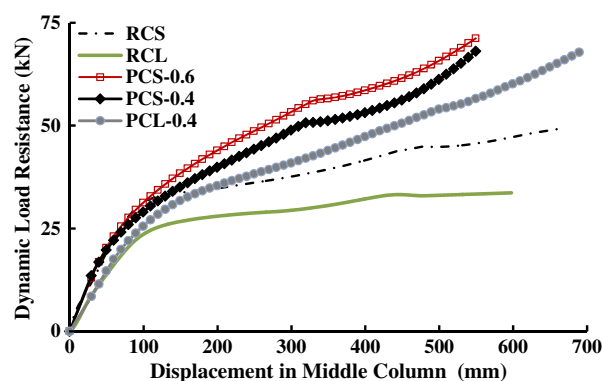


**Fig. 18.** Dynamic performance of the specimens

Although the effects of UPS on the quasi-static behavior of RC frames to resist progressive collapse have been quantified by test results, it is necessary to remember that removal of a column is dynamic in progressive collapse events caused by blast pressure, shock, or high-speed vehicular impact. Thus, it is necessary to quantify the effects of UPS on the dynamic behavior of RC frames subjected to a sudden column removal scenario. Single-degree-of-freedom (SDOF) models and capacity curve methods are frequently used to predict the dynamic response of RC frames based on measured load-displacement curves (Qian and Li 2015b; Tsai 2010). Previous studies (Qian and Li 2015b; Tsai 2010) have validated the accuracy of the capacity curve method. Thus, the capacity curve method, which was first proposed by Abruzzo et al. (2006), is used in this study, and it is mathematically expressed

$$P_{CC}(u_d) = \frac{1}{u_d} \int_0^{u_d} P_{NS}(u) du \quad (3)$$

where  $P_{CC}(u)$  and  $P_{NS}(u)$  = capacity function and nonlinear static loading estimated at the displacement demand  $u$ , respectively.

Fig. 18 illustrates the dynamic performance of tested specimens. As shown in the figure, the dynamic ultimate capacity of RCS, RCL, PCS-0.4, PCS-0.6, and PCL-0.4 is 49, 33, 68, 71, and 68 kN, respectively. Thus, UPS with  $0.4f_{pu}$  could increase the dynamic ultimate capacity of RCS and RCL by 39 and 106%, respectively. UPS with  $0.6f_{pu}$  could increase the dynamic ultimate capacity of RCS by 45%. Thus, UPS not only improve the quasi-static resistance of the frames, but also their dynamic resistance.

## Conclusions

Based on the experimental results and discussions, the main conclusions can be drawn as follows:

- Uniformly distributed design service loads could not be ignored in pushdown tests when evaluating the behavior of moment-resisting frames to resist progressive collapse. A uniformly distributed design service load may change the load-resisting capacity of the frames significantly;
- Unbonded posttensioning strands with a parabolic curve could significantly improve the behavior of RC frames to resist progressive collapse in the large deformation stage. This is because stretching of UPS could provide additional catenary action and increase the ultimate load capacity in the large deformation stage. The test results indicated that UPS could increase the maximum horizontal reaction force and ultimate load capacity by 124 and 191%, respectively. Furthermore, the UPS could



upgrade the dynamic ultimate capacity of RC subassemblages up by 106%;

- UPS will change the load-resisting mechanism of the frame. No reliable compressive arch action developed in PC subassemblages that could explain the upgrading of the first peak load in PC specimens' limit. In addition, UPS will aggregate the damage in the beam ends near the middle column, but they may lessen the damage in beam ends near the side column;
- Span/depth ratio has significant effects on the behavior RC subassemblages to resist progressive collapse. However, the effects on PC subassemblages are much milder, especially for the yield load capacity and initial stiffness; and
- Higher effective prestress in UPS may upgrade the initial stiffness and yield load capacity of the frames slightly. However, the lower effective prestress in UPS may delay the yielding and fracture of UPS and lead PC frames to achieve larger ultimate deformation capacity, which will result in the frame more effectively developing catenary action. Thus, it is suggested that PC frames be designed with proper effective prestress to balance the progressive collapse resistance and original purpose for gravity load resistance.

## Future Works

More tests should be carried out to study the progressive collapse behavior of PC frames with commonly used effective prestress in strands. To evaluate the effects of unbonded posttensioning strands on RC frames more accurately, a three-dimensional PC model with slabs should be carried out in the future. Dynamic tests should also be carried out because only a quasi-static pushdown test was carried out.

## Acknowledgments

This research was supported by a research grant provided by the Natural Science Foundation of China (Nos. 51568004, 51478118, 51678164, and 51568005). Any opinions, findings, and conclusions expressed in this paper are those of the authors and do not necessarily reflect the view of Natural Science Foundation of China.

## References

- Abruzzo, J., Matta, A., and Panariello, G. (2006). "Study of mitigation strategies for progressive collapse of a reinforced concrete commercial building." *J. Perform. Constr. Facil.*, [10.1061/\(ASCE\)0887-3828\(2006\)20:4\(384\)](#), 384–390.
- Choi, H., and Kim, J. (2011). "Progressive collapse-resisting capacity of RC beam-column sub-assembly." *Mag. Concr. Res.*, *63*(4), 297–310.
- DoD (U.S. Department of Defense). (2009). "Design of building to resist progressive collapse." *UFC 4-023-03*, Washington, DC.
- Ellingwood, B. R., Dusenberry, D. O., Duthinh, D., Lew, H. S., and Carino, N. J. (2006). "Best practices for reducing the potential for progressive collapse in buildings." *Rep. No. NISTIR 7396*, National Institute of Standards and Technology, Gaithersburg, MD.
- GSA (General Service Administration). (2003). *Progressive collapse analysis and design guidelines for new federal office buildings and major modernization projects*, Washington, DC.
- Kim, J., and Choi, H. (2015). "Monotonic loading tests of RC beam-column subassembly strengthened to prevent progressive collapse." *Int. J. Concr. Struct. Mater.*, *9*(4), 401–413.
- Kim, J., and Shin, W. S. (2013). "Retrofit of RC frames against progressive collapse using prestressing tendons." *Struct. Des. Tall Spec. Build.*, *22*(4), 349–361.
- Kim, J., and Shin, W. S. (2013). "Retrofit of RC frames against progressive collapse using prestressing tendons." *Struct. Des. Tall Special Build.*, *22*(4), 349–361.
- Lu, X., Lin, K. Q., Li, Y., Guan, H., Ren, P., and Zhou, Y. L. (2017). "Experimental investigation of RC beam-slab substructures against progressive collapse subject to an edge-column-removal scenario." *Eng. Struct.*, *149*, 91–103.
- Qian, K., and Li, B. (2013). "Performance of three-dimensional reinforced concrete beam-column substructures under loss of a corner column scenario." *J. Struct. Eng.*, [10.1061/\(ASCE\)ST.1943-541X.0000630](#), 584–594.
- Qian, K., and Li, B. (2015a). "Analytical evaluation of the vulnerability of RC frames for progressive collapse." *J. Perform. Constr. Facil.*, [10.1061/\(ASCE\)CF.1943-5509.0000493](#), 04014025.
- Qian, K., and Li, B. (2015b). "Quantification of slab influences on the dynamic performance of RC frames against progressive collapse." *J. Perform. Constr. Facil.*, [10.1061/\(ASCE\)CF.1943-5509.0000488](#), 04014029.
- Qian, K., and Li, B. (2015c). "Research advances in design of structures to resist progressive collapse." *J. Perform. Constr. Facil.*, [10.1061/\(ASCE\)CF.1943-5509.0000698](#), B4014007.
- Qian, K., Li, B., and Ma, J. (2015). "Load-carrying mechanism to resist progressive collapse of RC buildings." *J. Struct. Eng.*, [10.1061/\(ASCE\)ST.1943-541X.0001046](#), 04014107.
- Ren, P., Li, Y., Lu, X., Guan, H., and Zhou, Y. L. (2016). "Experimental investigation of progressive collapse resistance of one-way reinforced concrete beam-slab substructures under a middle-column-removal scenario." *Eng. Struct.*, *118*, 28–40.
- Sadek, F., Main, J. A., Lew, H. S., and Bao, Y. H. (2011). "Testing and analysis of steel and concrete beam-column assemblies under a column removal scenario." *J. Struct. Eng.*, [10.1061/\(ASCE\)ST.1943-541X.0000422](#), 881–892.
- Sasani, M., and Kropelnicki, J. (2008). "Progressive collapse analysis of an RC structure." *Struct. Des. Tall Special Build.*, *17*(4), 757–771.
- Su, Y. P., Tian, Y., and Song, X. S. (2009). "Progressive collapse resistance of axially-restrained frame beams." *ACI Struct. J.*, *106*(5), 600–607.
- Tsai, M. H. (2010). "An analytical methodology for the dynamic amplification factor in progressive collapse evaluation of building structures." *Mech. Res. Commun.*, *37*(1), 61–66.
- Yi, W., He, Q., Xiao, Y., and Kunnath, S. K. (2008). "Experimental study on progressive collapse-resistant behavior of reinforced concrete frame structures." *ACI Struct. J.*, *105*(4), 433–439.
- Yu, J., and Tan, K. (2013). "Structural behavior of RC beam-column subassemblages under a middle column removal scenario." *J. Struct. Eng.*, [10.1061/\(ASCE\)ST.1943-541X.0000658](#), 233–250.